Journal of Optics
https://doi.org/10.1007/s12596-024-02041-3

RESEARCH ARTICLE

Estimate of macronutrient concentration in dried flaxseed plants using laser-induced breakdown spectroscopy (LIBS) technique

Zainab Jameel Kamil[1] · **Muayyed Jabar Zoory**[1] · **Haidar J. Mohamad**[1]

Received: 14 May 2024 / Accepted: 1 July 2024

Abstract
Metal concentration percentage in plants has attracted scientists because of macronutrients that are involved in our lives. There are a lot of methods to measure these concentrations, but with low accuracy like atomic absorption spectroscopy (AAS). Laser-induced breakdown spectroscopy (LIBS) technique does not need advanced preparations for samples compared to AAS technique. Dried flaxseed plants are used to measure Fe, P, K, Mg, Al, and S concentration using LIBS and X-ray fluorescence (XRF) techniques. Metal concentrations depend on two parameters: electron temperature which is measured by spectral line equation and electron density determined using the McWhirter equation. A new equation used to measure metal concentration with high accuracy measurements depending on using two lines in the spectrum. The concentration of elements found in the dried flaxseed sample are Al (3.06%), S (1.6%), P (2.58%), Mg (1.17%), F (0.65%), and K (0.64%). There is an excellent agreement between the concentrations of the LIBS technique and the XRF technique.

Keywords Laser-induced breakdown · X-ray fluorescence · Macronutrient · Plants

Introduction

Micronutrient deficiencies, especially those associated with malnutrition in iron (Fe), phosphorus (p), potassium (K), sulfur(S), magnesium (Mg), and aluminum affect billions of people around the world [1]. Undernutrition is a pervasive issue that impacts both wealthy and less-developed nations. Technologies such as X-ray Fluorescence (XRF) and laser-induced breakdown spectroscopy (LIBS) are viable options for exploration because they allow rapid detection of different elements in plants. Combining these techniques with botany can enhance the characterization of mineral ratios in plants more efficiently [2, 3]. In order to create a database, researchers typically have difficulty and need a significant amount of time to collect several leaf samples as raw datasets. It is vital to identify and categorize plants according to their respective roles through available technologies [4, 5].

There are many techniques to analyze the plant's materials. One of the powerful analytical techniques is XRF. It is high-energy electromagnetic radiation that lies between gamma rays and ultraviolet rays [6]. There are two types of measurement of photon energy: Wavelength Dispersive X-ray fluorescence Analysis (WD-XRF) and Energy Dispersion X-ray fluorescence (ED-XRF) [7].

Among the previous studies in which laser-induced plasma met the necessary condition for local dynamic equilibrium (LTI) in its experiments can be summarized as: Andrade et al. (2018) used LIBS to study sugarcane leaves to determine the concentrations of microelements such as calcium, potassium, magnesium, phosphorus, boron, copper, iron, manganese, and zinc. The output of this work was to understand the effect of these minerals on leaf formation and plant health [8].

Rehan et al. (2021) used the LIBS technique to verify the essential elements found in dry fruits quantitatively. Pistachios, cashews, white walnuts, black walnuts, and almonds were examined using LIBS technique. It showed that the experimentally measured electron density is greater than the expected critical electron density [9].

✉ Zainab Jameel Kamil
zainab.jameel@uomustansiriyah.edu.iq

Muayyed Jabar Zoory
Muayyedjz@uomustansiriyah.edu.iq

Haidar J. Mohamad
haidar.mohamad@uomustansiriyah.edu.iq

[1] Department of Physics, College of Science, Mustansiriyah University, Baghdad, Iraq

Published online: 13 July 2024

Iman et al. (2023) studied the potential of LIBS technique to identify kidney failure in patients with iron deficiency. They observed statistically significant differences in the initial composition of blood samples among kidney failure patients, unlike healthy individual patients. This study focused on the benefit of LIBS in the Department of Kidney Health [10]. In (2024), Zainab et al. presented a survey on the principles of LIBS technique and its efficiency to detect the proportions and concentrations of plant minerals and elemental compositions within plant tissues by comparing the LIBS tool with other analytical tools [8].

This work aims to find the percentages of metal concentrations in dried flaxseed plants using the LIBS technique and compare it with XRF technique. It highlights the need for an accurate and reliable analytical tool in determining element profiles and distinguishing between micro- and macronutrients. There is a new equation used to calculate the concentration of metals. This equation depends on measure the concentration of metals using two lines in the spectral lines instead of one line.Keyword: Laser-induced breakdown, X-ray fluorescence, macronutrient, plants

Methodology

There is an analytical technique to measure the plant's elements in a short time compared with other methods. The fastest and most accurate technique is LIBS, which depends on a high-pulsed laser with different wavelengths. The high energy generates the atomic emission of the tested material [11]. This emission is related to the ionized plasma that is generated at the sample surface, which is formed by projecting a laser pulse on the surface of the target. This reaction produces a cloud of plasma on the surface of the sample [12, 13]. Through the process of ionization of photons, the electronic seeds are formed to form a careful plasma so that these electronic seeds allow the laser energy to be absorbed [14]. Ionization is increased through the reverse bremsstrahlung process, so the increase in the rate of ionization causes the increase in the absorption of the laser beam and thus leads to the ionization of the skin collapse until it reaches the plasma [15, 16]. Then, the plasma reaches a critical density, and a large part of the laser is reversed; therefore, electron density (*Ne*) decreases due to the expansion of the plasma. The laser penetrates the plasma, which causes the surface of the target to heat. The composition of the plasma and ionization processes affect the transfer of energy to the form of plasma [17, 18]. The ionized gas is made up of positively and negatively charged particles with about equal charge densities [19–21]. The spectra lines of these emissions show the sample components precisely [22, 23].

Sample preparation

The sample of flax seeds plants was brought from orchards located in Baghdad-Iraq. The sample weight was 20 mg before putting them in the oven as shown in Fig. 1 (a). It is necessary to wipe the floor of the oven with ground detergents (Ethanol C_2H_6O, Acetone C_3H_6O). The temperature adjusted between 45 and 55 C°. The sample is left inside the oven for about one hour and the nozzle opens so that we get rid of liquid materials. The sample is let to be dried and cooled by closing the oven nozzle. The sample is grinded by a 2 ml ceramic hand grinder to remove the crustacean material, then grind it with an electric grinder. The resulted grind sample sieved with a 2mL with 38 micros sieve to get rid of cellulose and large molecules. The tested sample is weighted as 5 mg because the pellet holder with this size under a 5-ton piston mold. The resulting coherent sample with diameter 1.5 cm according to the mold used as shown in Fig. 1 (b).

LIBS setup

Experimental setup chosen to be at room temperature, about 25 ºC. The laser system in LIBS used a single-pulse laser (Q-Switched Nd: YAG) with wavelength 1064 nm and energy 10 mJ. The laser pulse duration is 10 nanoseconds for one pulse. The setup consists of lenses and optical fibers

Fig. 1 Sample (**a**) dried flax seeds preparation and (**b**) before measure by LIBS technique

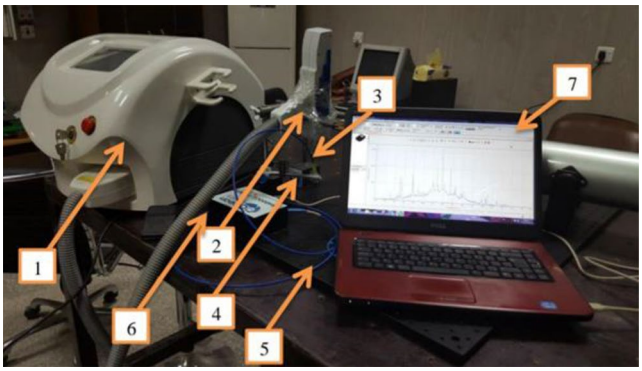

Fig. 2 Schematic of the LIBS setup: LIBS System (1) Nd: YAG laser system, (2) Laser handle, (3) target holder, (4) Lens, (5) Fiber optics cable, (6) Spectrometer (spectrum analyzer), and (7) Computer

Fig. 3 XRF system used for experiment

to collect and transmit light. A Convex lens (quartz-silica) was used to focus the laser beam at a focal length (10 cm) on the surface of the sample placed on a moving platform of variable height.

The spectroscopy device is used to determine the elements and their relative concentrations. This is done by collecting light emissions from plasma and directing them to the spectrometer. Spectrum analyzer model (BIM_6002) used to determine the resulting spectral lines. The spectrometer transmits the digital signal to an operating system (OOIBase32- Spectrometer) from Ocean Optical Corporation (Ocean Optic, Inc.), which is then analyzed by computer software. The emission wavelengths from the sample are recorded in the range (187–915 nm). Figure 2 shows the experimental setup for the tested samples.

EDXRF analysis

EDXRF depends on transition of electron from the inner shell by X-ray source. Thus, the detector generates a single package of X-rays focusing on the target material for irritating energy levels and, thus, the movement between higher energy levels. Hence, the occurrence of decay and the emission of different spectrums, the detector contains the number of silicone reagents that are described by the location of a different irritation energy, which results in high-energy rays falling in distant beginnings on the detector surface. Figure 3 shows the device that was used for experimental setup.

Method and material

It is assumed that laser-induced plasma is present in the state of LTE, and the plasma must have enough humidity to ensure a high collision rate LTE. To achieve this condition, the temperature of the plasma and the number of electron densities must be determined. The temperature is determined by describing the energy levels in the thermal equilibrium through one spectral line as [24, 25]:

$$T\,(ev) = -\frac{Ek}{K * Ln\,(I * \lambda\,/Ak * gk)} \tag{1}$$

where *Ek* is the energy level excited, *Ak* is the transition probability, *gk* the statistical weight for the higher level, *K* Boltzmann constant, and *I* is intensity.

Electron density *(Ne)* is determined by the McWhirter criterion and is given by the following relationship [8]:

$$Ne \geqslant 1.6 * 10^{12} * T^{1/2} * (\Delta E)^3 \tag{2}$$

where *T* is the plasma temperature, ΔE is the highest energy transition.

The highest and lowest intensity of each element was taken to calculate the average of *Ne* and the temperature rate of each component in the sample to find the concentration ratios of the six metals. It is also shown that electron density affects the atomic interaction and the arrangement of electrons in atomic orbitals. These variables affect the concentrations measured in the sample.

The reason for finding the metal concentration (*C*) is that it is a necessary and vital factor to find the amount of element present in the sample and it is high or not, and the concentration equation is used in this work through the electron density of each element as:

$$C = \frac{ne1}{ne2} \tag{3}$$

where *ne1* is the electron density of the first line of the element, and *ne2* is the electron density of the second line of the element.

Table 1 Fe data of NIST and LIBS technique for the tested sample

Sample	Intensity (a .u.)LIBS	Wavelength (nm) LIBS	Wavelength (nm) NIST	Aki(s-1) Transition Potential	gk	Ei (ev) lower-level energy	Ek (eV) higher level energy
Fe I	3486	655.426	655.45466	1,870,000	8	11.05024911	12.94125345
Fe II	6312	769.174	769.1507	3,300,000	4	11.3535	12.9650556
Fe II	20,865	769.915	769.9265	9,600,000	6	11.3868	12.99670048

Table 2 Mg data of NIST and LIBS technique for the tested sample

Sample	Intensity (a .u.)	Wavelength (nm) LIBS	Wavelength (nm) NIST	Aki(s-1) Transition Potential	gk	Ei (eV) lower-level energy	Ek (eV) higher level energy
mg I	1394	706.042	706.0409	851,000	7	5.75309840	7.508616298
mg I	1725	571.141	571.10880	3,860,000	7	4.34569076	6.515970976
mg II	1223	678.126	678.1451	2,490,000	4	12.08258	13.91031733

Table 3 P Data of NIST and LIBS technique for the tested sample

Sample	Intensity (a.u.)	Wavelength (nm) LIBS	Wavelength (nm) NIST	Aki(s-1) Transition Potential	gk	Ei (eV) lower-level energy	Ek (eV) higher level energy
P I	803	515.488	515.4844	1.5e + 06	6	6.9541719	9.358638711
P I	2529	547.733	547.7672	5,700,000	6	7.21251607	9.475275697
P II	2951	608.788	608.782	2.70E + 07	3	10.7546029	12.79057549
P II	556	453.031	453.081	18,000,000	5	13.05583	15.791524
P II	988	534.453	534.475	32,000,000	3	10.7364508	13.05549313

Table 4 AL data of NIST and LIBS technique for the tested sample

Sample	Intensity (a.u.)	Wavelength (nm) LIBS	Wavelength (nm) NIST	Aki(s-1) Transition Potential	gk	Ei (eV) lower-level energy	Ek (eV) higher level energy
Al I	1103	690.603	690.64	1,150,000	8	4.021546405	5.816243785
Al II	2967	606.61	606.637	888,000	3	15.584801	17.62798308
Al II	1365	705.674	705.660	57,400,000	3	11.3163038	13.07274261
Al II	1620	597.18	597.198	5,810,000	5	15.6053663	17.6808399
Al III	2744	605.521	605.521	8,590,000	4	23.41723	25.46418111

Table 5 K data of NIST and LIBS technique for the tested sample

Sample	Intensity (a.u.)	Wavelength (nm) LIBS	Wavelength (nm) NIST	Aki(s-1) Transition Potential	gk	Ei (eV) lower-level energy	Ek (eV) higher level energy
K II	3302	612.057	612.027	168,000,000	7	21.08286987	23.10804991
	2464	547.015	547.013	20,700,000		20.44792597	22.71382752
K II	2423	548.812	548.806	26,300,000	3	24.14805213	26.40653962

Results and discussions

The wavelength values recorded in the sample ranged from 187.786 nm to 915.914 nm. There is a matching between the values measured by the LIBS technique and the values approved by NIST. NIST has important parameters to measure the electron temperature like *gk* and *Ek*. *gk* is the change in quantum momentum and its value between 1 and 10 in the elements. *Ek* represents the energy of the highest level, which changes in terms of the lines of elements and from element to element, and this interpretation indicates a difference in the structure and order of the energies of the electronic levels in the atoms of the element. Table 1 represents the comparison between the Fe data of NIST and experimental data of LIBS technique. The data of Mg, P, Al, K, and S are represented in Tables 2, 3, 4 and 5, and 6, respectively. Figure 4 shows the spectrum of LIBS technique for the tested sample.

The electron temperature of the sample elements is shown in Table 7, which relates to calculating the electron density for each line of the sample's wavelengths.

Table 6 S data of NIST and LIBS technique for the tested sample

Sample	Intensity (a.u.)	Wavelength (nm) LIBS	Wavelength (nm) NIST	Aki(s-1) Transition Potential	gk	Ei (eV) lower-level energy	Ek (eV) higher level energy
S I	2326	641.547	641.550	1.61e+06	5	7.8697003	9.801694857
S I	1167	772.508	772.50461	1.38e+00	1	1.14541198	2.749892877
S I	1385	699.422	699.458	1,550,000	3	8.04544721	9.817478878
S II	341	708.986	708.9567	59,000,000	2	33.60144	35.34974
S II	2258	566.452	566.478	38,900,000	2	13.6598571	15.84788124
S II	2228	639.723	639.7359	14,900,000	4	14.1624786	16.09994701
S IV	1414	708.986	708.9567	59,000,000	2	33.6014422	35.34973548

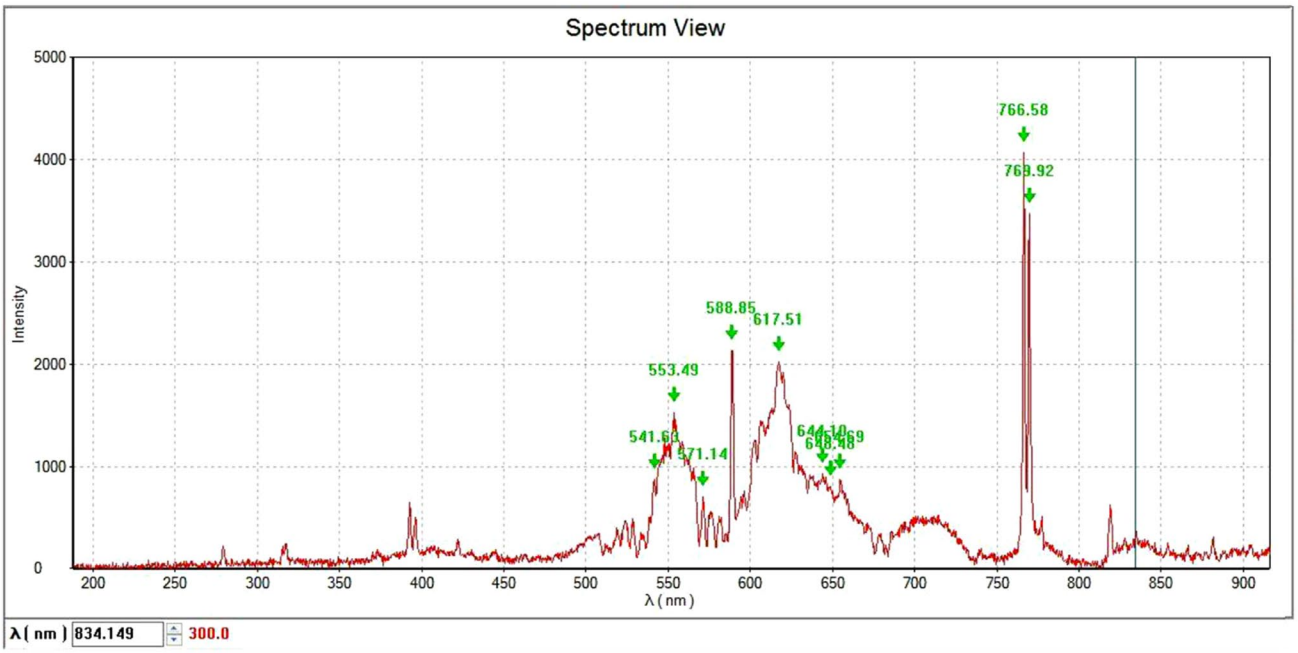

Fig. 4 Spectra of the studied samples using LIBS technique

Table 7 Plasma temperature with element

Elements	temperature (Te1) (K)	temperature (Te2) (K)
Fe	6855.680614	6002.621514
Mg	3423.343125	6955.45104
P	6872.450536	6050.671628
Al	12441.30601	2907.534136
K	9899.324249	12353.52672
S	5076.088488	7207.372015

The temperature of the elements for the tested sample is shown in Fig. 5. The behaviour is as expected according to the percentage for each element.

Aluminum has the highest temperature among the elements, followed by phosphorus, iron, sulfur, magnesium, then potassium. Electron density (*Ne*) is related to the element temperature (*T*). So, there is a proportional relationship between *T* and *Ne*. The amount of concentration also depends on the temperature of the component.

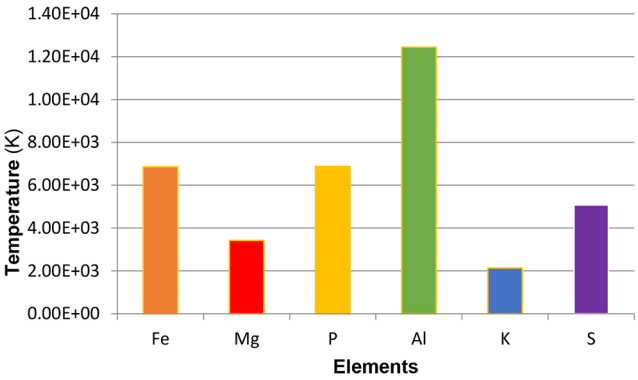

Fig. 5 Elements and temperature of the sample

Table 8 shows the concentration of each element depending on the new equation that we presented in this work. This equation depends on low and high intensity of λ for the selected element. This equation gives high accuracy in concentration compared with XRF. There is a small difference

Table 8 First-line electron density (ne1), second-line electron density (ne2) and concentration of the sample

Element	First line electron density (ne1)	second line electron density (ne2)	Concentration %
Al	1.53065E + 16	4.98719E + 15	3.06
S	8.22058E + 15	5.11409E + 15	1.60
P	2.71568E + 16	1.05036E + 16	2.58
Mg	9.56957E + 15	8.14745E + 15	1.17
Fe	5.52719E + 15	8.40166E + 15	0.65
K	1.32225E + 16	2.04865E + 16	0.64

Table 9 XRF analysis sample

Element	Content	Detection limit	Error
Al(%)	3.13	0.00	0.15
P(%)	2.57	0.00	0.03
S(%)	1.50	0.00	0.01
Mg(%)	1.24	0.00	0.07
K(%)	0.69	0.00	0.00
Fe(%)	0.62	0.00	0.01
Ti(%)	0.12	0.00	0.00
W(%)	0.08	0.00	0.01
Zr(%)	0.06	0.00	0.00
Ba(%)	0.06	0.00	0.00
Ni(%)	0.05	0.00	0.00
Cu(%)	0.04	0.00	0.00
Zn(%)	0.04	0.00	0.00
Sr(%)	0.03	0.00	0.00
Rb(%)	0.02	0.00	0.00
Ag(%)	0.01	0.00	0.00
Cd(%)	0.01	0.00	0.00
Si(%)	0.00	0.00	0.00
Ca(%)	0.00	0.00	0.00
V(%)	0.00	0.00	0.00
Cr(%)	0.00	0.00	0.00
Mn(%)	0.00	0.00	0.00
Co(%)	0.00	0.00	0.00
As(%)	0.00	0.00	0.00
Se(%)	0.00	0.00	0.00
Sn(%)	0.00	0.00	0.00
Sb(%)	0.00	0.00	0.00
Mo(%)	0.00	0.00	0.00
Ta(%)	0.00	0.00	0.00
Au(PPM)	0.00	0.00	0.00
Hg(PPM)	0.00	0.00	0.00
Pb(%)	0.00	0.00	0.00

in presenting the elements in Tables 8 and 9 regarding the micronutrient. In Table 8, we presented only the elements that are involved with micronutrients, while Table 9 shows all the elements even with low concentrations.

It is important to point out that the McWhirter equation is satisfied with the resulted data. The laser-induced plasma is located in LTE equilibrium, the expected critical electron density was 2.715E + 16 cm^{-3}. This is less than

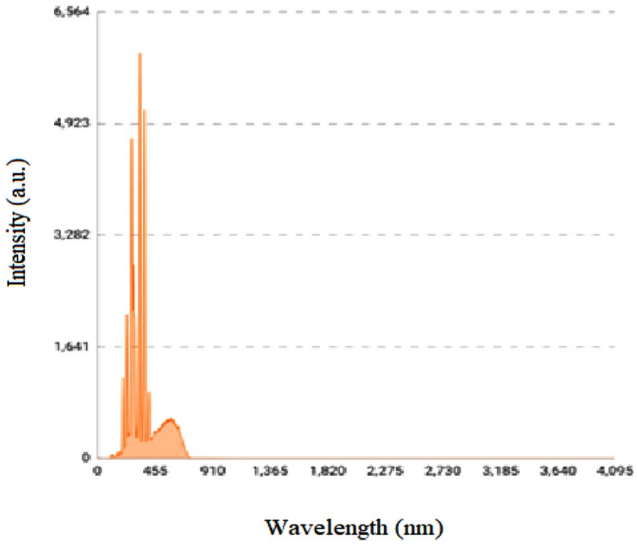

Fig. 6 XRF spectrum of the sample

Table 10 Comparison between LIBS and XRF

Element	Concentration of LIBS	Concentration of XRF	Error between two methods %
Fe	0.65%	0.62% ± 0.01	4.83871
Mg	1.17%	1.24% ±0.07	5.645161
P	2.58%	2.57% ±0.03	0.389105
Al	3.06%	3.13% ±0.15	2.236422
K	0.61%	0.64% ±0.00	4.6875
S	1.60%	1.50% ±0.01	6.666667

the experimentally calculated electron density. This means laser-induced plasma does met the requirement for LTE in our experiments [17].

The high concentration in Table 8 is about 3% for Al element. This is because of the sample origin and the environment that affected the element percentage. The other findings of flaxseed concentrations are different with ours data which are Fe (5.73 mg), Mg (392 mg), P (642 mg), and K (813 mg) in each 100 mg [26].

Figure 6 shows the spectrum of the XRF for the tested sample, and it shows the elements wavelength between 187 and 915 nm. And Table 9 shows the concentrations of elements in the laboratory sample with the percentage of error of the XRF device. The table shows that the highest concentration among the element concentrations is aluminum.

The comparison between LIBS technique and XRF data for element concentration is shown in Table 10. There is a small difference between the two methods which gives good indication for the resulting data. There is a strong agreement between the results of the XRF and LIBS tests using the weight ratios that were employed, indicating that the electron density essentially determines the presence of

microscopic difference element characteristics like reactivity and bonding behavior.

Conclusion

XRF and LIBS technique used to analyze essential minerals in dried flax seeds. The local thermodynamic equilibrium of the laser-polluted plasma was established and verified using the McWhirter criterion based on the electron number density in the plasma.

There is a direct relationship between temperature, electron density, and concentration. The high concentration component of the dried flax seeds sample is the aluminum (Al) element at a concentration of (3.03%), followed by P (2.56%), S (1.60%), Mg (1.17%), Fe (0.65%), and K (0.64%).

There is a good agreement between XRF and LIBS technique data. Laser-induced plasma does meet the requirement for LTE in our experiment.

References

1. F.-J. Zhao et al., Variation in mineral micronutrient concentrations in grain of wheat lines of diverse origin. J. Cereal Sci. -J. CEREAL SCI. **49**, 290–295 (2009)
2. P.R. Shewry, Wheat, J. Exp. Bot. **60**(6), 1537–1553 (2009)
3. L.A. Berner, D.R. Keast, R.L. Bailey, J.T. Dwyer, Fortified foods are major contributors to nutrient intakes in diets of US children and adolescents, (in eng). J. Acad. Nutr. Diet. **114**(7), 1009–1022 (2014)
4. L. Ge, F.J.X.R.S. Li, Review of in situ X-ray fluorescence analysis technology in China, **49** (4), 458–470, (2020)
5. A.N. Abd, S.K. Rahi, Z.M.A.J.N. Khalik, The effect of x-rays in some optical properties of the thin film polystyrene (ps) dissolved in phenyl methane (toluene), **18**(6), 21, (2020)
6. K. VanEvery et al., Column formation in suspension plasma-sprayed coatings and resultant thermal properties, **20**, 817–828 (2011)
7. A. Khalid, A.T. Khan, J. o. P. Anwar, X-Ray fluorescence (XRF) spectrometry for materials analysis and discovering. At. Number. **64**, 335–338 (1996)
8. Z.J. Kamil, M.J. Zoory, H.J. Mohamad, LIBS technique for plant mineral ratio analysis and environmental and agricultural importance: a comprehensive review. Eur. Phys. J. D **78**(3), 27 (2024)
9. I. Rehan et al., Nutritional and toxic elemental analysis of dry fruits using laser induced breakdown spectroscopy (LIBS) and inductively coupled plasma atomic emission spectrometry (ICP-AES), **28**(1), 408–416, (2021)
10. I. Sami, M.J. Zoory, S.H. Lefta, Implementation of laser-induced breakdown spectroscopy (LIBS) technique in evaluating of renal failure in patients with iron (Fe) deficiency. Advancements Life Sci. **11**(1), 66–77 (2024)
11. Q. Abbas, A.F. Adnan, Ahmed, A.-H. Falah, Mutlak, Spectroscopic analysis of magnetized hollow cathode discharge plasma characteristics. Optik. **242**, 167260 (2021)
12. A.F. Ahmed, A.-H. Falah, Mutlak, and Qusay Adnan Abbas. Evaluation of cold plasma effect to achieve fullerene and zinc oxide-fullerene hydrophobic thin films. Appl. Phys. A **128**(2), 147 (2022)
13. A.F. Ahmed et al., Plasma parameters of au nano-particles ablated on porous silicon produced via Nd-YAG laser at 355 nm for sensing NH3 gas. Optik,**249**, 168260, (2022)
14. A.F. Ahmed, W.I. Yaseen, Q.A. Abbas, F.A. Mutlak, (2021). Plasma treatment effect on SnO 2–GO nano-heterojunction: fabrication, characterization and optoelectronic applications, Applied Physics A, 127, 1–16, (2021)
15. A. Ghasemi, V. Raja, C. Blawert, W. Dietzel, and K. *Kainer,the role of Anions in the Formation and Corrosion Resistance of the Plasma Electrolytic Oxidation Coatings*, vol. 204 (Surface & Coatings Technology - SURF COAT TECH, 2010), pp. 1469–1478
16. X. Jiang, P. Hayden, J. Costello, E. Kennedy, Double-pulse laser Induced Breakdown Spectroscopy with Ambient Gas in the Vacuum Ultraviolet: optimization of Parameters for Detection of Carbon and Sulfur in Steel. Spectrochimica Acta Part. B: at. Spectrosc., **101**, (2014)
17. S. Yao, M. Dong, J. Lu, J. Li, X.J.L.P. Dong, Correlation between grade of pearlite spheroidization and laser induced spectra, **23**, 12, p. 125702, 2013
18. J.J. Chang, B.E. Warner, Laser-plasma interaction during visible-laser ablation of methods. Appl. Phys. Lett. **69**(4), 473–475 (1996)
19. V. Balaram, Advances in Analytical techniques and applications in exploration, mining, extraction, and Metallurgical studies of Rare. Earth Elem. Minerals. **13**(8), 1031 (2023)
20. D.A. Cremers, L.J. Radziemski, *Handbook of laser-induced Breakdown Spectroscopy* (Wiley, 2013)
21. M. Abdul-Hussain, H. Mohamad, Thermal effect in a 3-D Simulation within Multilayer Thin Film of Ultrafast-Pulsed laser. Al-Mustansiriyah J. Sci. **32**, 104–109 (2021)
22. N. Schlatter, B. Lottermoser, Laser-Induced Breakdown Spectroscopy Applied to Elemental Analysis of Aqueous solutions – a Comprehensive Review. Spectrosc. J. **2**, 1–32 (2024)
23. S.K.R. Rahi, M.J.Z. Zoory, A.H. Ali, Design and develop an optical setup related to the pump-probe technique for spectroscopic study. Baghdad Sci. J. (2023)
24. H. Mohamad et al., Thermally induced magnetization dynamics of optically excited YIG/Cu/Ni81Fe19 trilayers, 96, 134431, (2017)
25. T.A. Gomez et al., Effect of Electron capture on Spectral Line broadening in hot dense plasmas, (in eng). Phys. Rev. Lett. **124**(5), 055003 (2020)
26. U.S. DEPARTMENT OF AGRICULTURE, Agricultural Research Service, https://fdc.nal.usda.gov/fdc-app.html#/food-details/169414/nutrients